p-ISSN 2089 – 0133 e-ISSN 2477-6416
URL: https://jurnal.uns.ac.id/ijap/article/view/99701
Indonesian Journal of Applied Physics (IJAP) Vol. 15 No.2 page 293
DOI: https://doi.org/10.13057/ijap.v15i2.99701

INFLUENCE OF CONCENTRATION TO THERMAL DIFFUSIVITY IN LIQUID FORM USING PHOTOPYROELECTRIC (PPE) SETUP AND DUAL-BEAM MODE-MISMATCHED THERMAL LENS METHOD WITH DIFFERENT OPTICAL SENSORS

Ting Lee Mon, Nor Kamilah Sa'at*, Raba' Ah Syahidah Azis, Md Shuhazlly Mamat@Mat Nazir, Nur Quratul Aini Ismail
Department of Physics, Faculty of Science, Universiti Putra Malaysia, Malaysia
*kamilah@upm.edu.my

Received 2025-02-20, Revised 2025-02-28, Accepted 2025-08-13,
Available Online 2025-10-1, Published Regularly October 2025

ABSTRACT

This study examines the effect of concentration on thermal diffusivity in nano-liquid formulations using the thermal lens method. Standard liquids and nano-liquid samples with varied concentrations were prepared and analyzed. Results showing an average trend of thermal diffusivity by using standard liquids, such as distilled water, ethylene glycol and glycerol and graphene oxide (GO). Thermal lens method with different optical sensors such as PVDF and photodiode also studied to examine the effect of sensor in thermal diffusivity measurement. Results indicate an increase in thermal diffusivity with rising GO concentration up to a threshold, beyond which further increments yield diminishing returns. This behavior is attributed to the unique thermal transport mechanisms enabled by GO nanosheets. These findings offer insights for optimizing GO-based nano-liquids for thermal management applications. Moreover, the study underscores the efficacy of the thermal lens method for probing thermal properties in nanofluid systems.

Keywords: thermal diffusivity; graphene oxide; concentration

INTRODUCTION

Thermal lens spectrometry (TLS) is first explained by [1]. According to [2], thermal lens spectrometry (TLS) is one of the precise photothermal methods, which is based on the temperature slope due to retention of optical radiation and non-radiative relaxation of the excited atoms. It is proven in the paper published by Shahriari et.al (2016) that the mode-mismatched thermal lens method provides larger signal-to-noise output. Thermal lens (TL) method is one of the effects of photothermal. Thermal lens method is a method that is using a laser with a Gaussian intensity profile as an excitation laser beam that induces the beam temperature in a laser [3]. According to Shahriari et. al (2016)[3], the heat produced is the strongest at the center as the concentration of the beam is the highest at the center. This temperature gradient by the heat produces a refractive index gradient which behaves like a converging or diverging lens depending on the change rate of refractive index with respect to temperature, dn=dT, is positive or negative [4], [5]. The thermal lens method is very sensitive which makes it suitable for measuring thermal diffusivity of nanofluid [2]. The thermal lens method can be used to measure low optical absorption coefficients of transparent samples either in gasses or fluids [5].

The dual-beam mode-mismatched thermal lens (DBMMTL) method is a powerful tool for characterizing the thermal and optical properties of materials. The DBMMTL method has been widely used for investigating the thermal diffusivity and optical properties of various materials, including liquids, polymers, and thin films. Advances in laser technology, such as the use of ultrafast lasers, have improved the temporal resolution of the thermal lens technique, allowing for more precise measurements of rapid thermal dynamics [6]. One of the notable areas of application for the DBMMTL method is in the study of nanostructured materials. The DBMMTL method's ability to probe small volumes with high sensitivity has proven particularly valuable in these studies, leading to new insights into the thermal behavior of nanoscale systems [7].

The PVDF materials is that they have relatively low charge sensitivity and voltage sensitivity, which is caused by piezoelectric coefficients [8]. Pyroelectricity is the ability of materials to generate a temporary voltage when they are heated or cooled [9]. The temperature change modifies the positions of the atoms slightly within the crystal structure so that the polarization of the material changes. This polarization change gives rise to a voltage across the crystal. According to Hammes (1992), the pyroelectric (PE) property of PVDF film makes it able to identify the temperature changes but not the steady temperature. The sensor senses the output signal in the form of voltage which it is further used as to identify defects like cracks, impact damages, and delamination.

Photodiode sensors are widely utilized in diverse applications, including optical communication, medical diagnostics, and environmental monitoring. A critical development which is the enhancement of photodiode materials to increase efficiency and broaden spectral sensitivity. For instance, researchers have explored the use of perovskite materials, which offer superior light absorption properties and faster response times compared to traditional silicon-based photodiodes [10]. Another significant trend is the integration of photodiodes into wearable and flexible electronics. Advances in organic photodiode technology have enabled the development of lightweight, flexible sensors that can be integrated into textiles or worn directly on the skin. This has opened new possibilities for continuous health monitoring and wearable optical devices.

British Chemist, B. C. Brodie (1859) discovered a highly oxidized form of natural graphite, named “graphon” which is currently known as “graphite oxide” or “graphene oxide”. However, it has been re-emerged as a material of interest after the groundbreaking discovery of graphene and its diverse methods of synthesis [11]. Graphite oxide can be considered as a highly oxidized form of graphite with a higher inter-layer spacing due to the presence of a large number of oxygen functionalities [12]. The GO is a non-stoichiometric macro-molecule having controlled physical and chemical properties depending on the synthetic variables such as graphite precursor, type of the oxidant and the dose, stirring or sonication strength, oxidation temperature and duration. The most acceptable structural model proposed for GO is Lerf-Klinowski model in which, basal planes of GO are decorated by hydroxyl and epoxide groups, whereas the edges are mainly occupied by carboxyl and carbonyl groups in a random manner resulting in mixed sp^2-sp^3 carbon containing sheets [13].

The oxidized form of graphene named “Graphene oxide” (GO) is produced by the oxidation of bulk graphite powders via chemical oxidation processes. Graphene oxide have a mixed structure bearing a variety of oxygen-containing various functional groups like epoxy (> O), hydroxyl (eOH), carbonyl (C=O) and carboxylic (eCOOH) groups[7] .

In this study, the experiment begins with distilled water, follow by Ethylene glycol (TianJin DaMao Reagent Factory, purity 99.9%) and lastly glycerol (TianJin Deng Ke Chemical Factory, purity 99.9%). Each of the samples withdraw 1ml using dropper and measuring cylinder. Whereas, fort the powdered Graphene Oxide, it is diluted with distilled water to different concentrations of the nano-liquid with a ratio of 1g to 100ml of distilled water. In this study, the nano-liquids used were 0.5g/ml, 1.0g/ml, 1.5g/ml, 2.0g/ml and 2.5g/ml [14].

Experimental Procedure

The GO nano-liquids prepared by measuring the ratio of GO powder to distilled water in fixed ratio of 1g to 100ml. The solutions prepared are in varied concentrations 0.5g/ml, 1.0g/ml, 1.5g/ml, 2.0g/ml and 2.5g/ml. The prepared solutions are then stirred using magnetic stirrer for 60 minutes, and the solution is maintained at 25°C before placing the solution for thermal diffusivity testing by using PPE setup and dual-beam mode-mismatched thermal lens method [14].

Prior to the study, the beam profiling of thermal lens was performed to optimize the laser source for probe beam and excitation beam as well as to achieve the maximum outpower by PPE and dual-beam mode-mismatched thermal lens method. This comparison is crucial to validate the both setups in determining the thermal diffusivity values of standard liquids and GO nano-liquid with different concentration.

In this study, the higher power laser of the blue laser (λ=473nm) was used as excitation laser whereas the slightly lower power laser of the green laser (λ=543nm) was as the probe beam laser. The output signal of the system was detected by PVDF sensor and photodiode sensor. The output signal detected will then transferred to the lock-in amplifier to be lock-in before analysis is done. The default settings of the lock-in amplifier were set as 100 ms sensitivity, and 300 ms time constant. The reason to set the setting of lock-in amplifier to 100ms sensitivity is because there is no any pre-amplifier connected to the setup. So, in order to obtain maximum output signal, the sensitivity has to be set at lower sensitivity values although the graphs will be more fluctuated. The optical arrangement of the thermal lens setup is as was shown in the Figure 1 and Figure 2. The experiment to determine the thermal diffusivity of the nano-liquids is repeated 3 times and an average value of the thermal diffusivity is obtained. The experimentally obtained data is then compared to theoretical thermal diffusivity values.

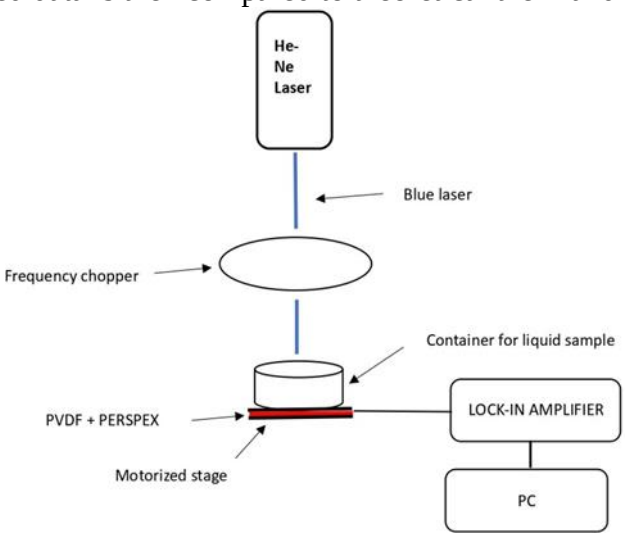

Figure 1 Schematic diagram of the PPE setup.

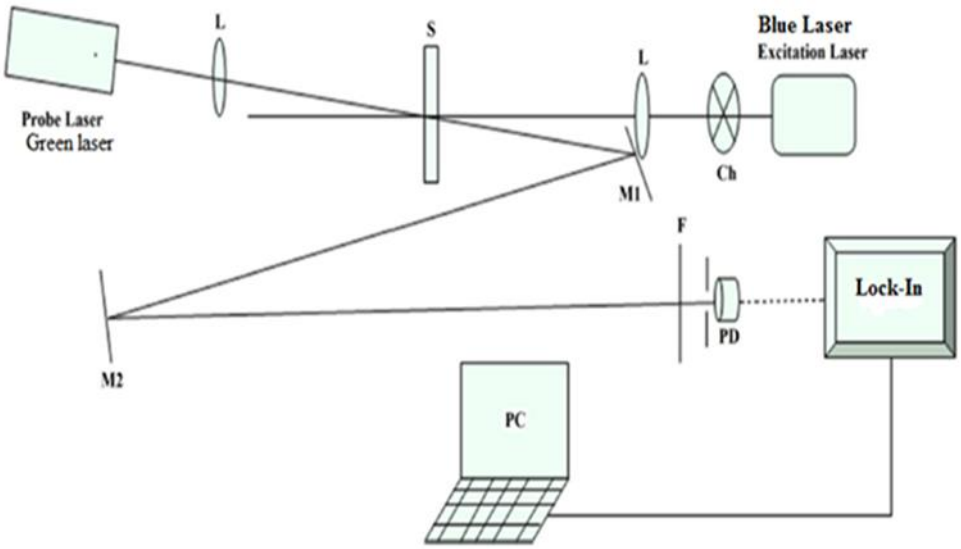

Figure 2 Schematic diagram of the dual-beam mode-mismatched thermal lens method setup

RESULTS AND DISCUSSION

Beam Profiling

Before starting the thermal diffusivity measurement, the beam profile is optimized to achieve the smallest beam size. This optimization uses two laser sources: a green laser (MGL- III-532, 150mW, 543nm) and a blue laser (MBL-III-473, 100mW, 473nm). The laser beam is evaluated at a constant frequency of 5Hz, with the x-axis and y-axis controlled by a motorized stage. The stage moves from 0 mm to 5 mm along the x-axis in 0.01 mm increments, and then along the y-axis. A PVDF sensor detects the output signal, which is then sent to a lock-in amplifier (SR530). The time constant is set at 3 seconds, and the lock-in amplifier sensitivity is fixed at 500 mV. The data is then transferred to a PC for further analysis. A Gaussian graph of the beam profile along the x-axis and y-axis is plotted as shown in Figure 3, Figure 4, Figure 5 and Figure 6.

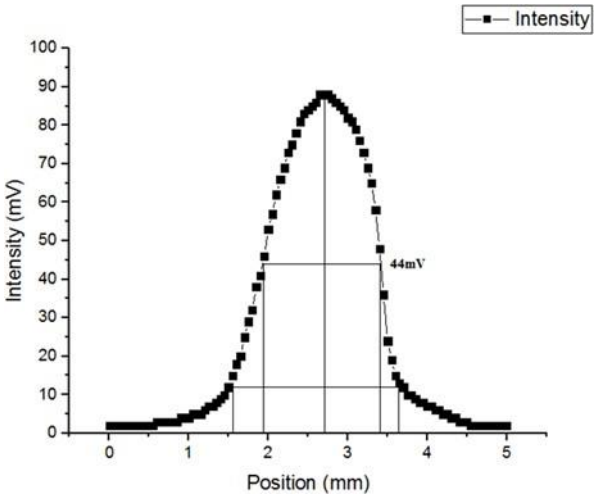

Figure 3 Intensity (mV) against position (mm) for green laser using PPE setup.

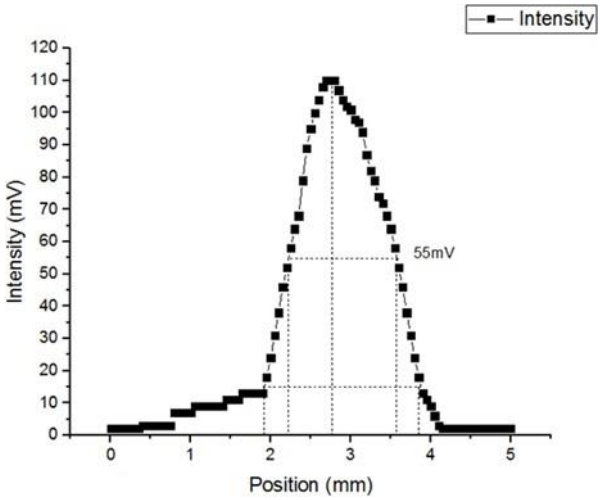

Figure 4 Intensity (mV) against position (mm) for blue laser using PPE setup.

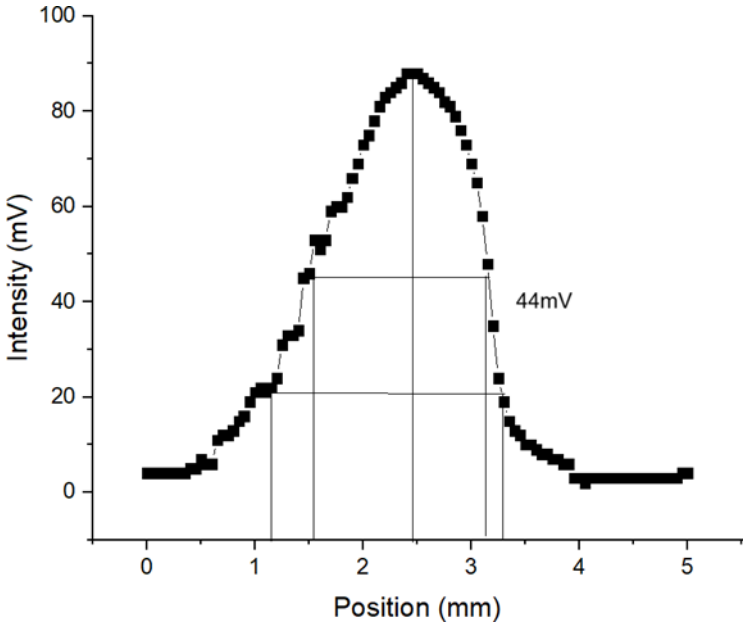

Figure 5 Intensity (mV) against Position (mm) for green laser using dual-beam mode-mismatched thermal lens method.

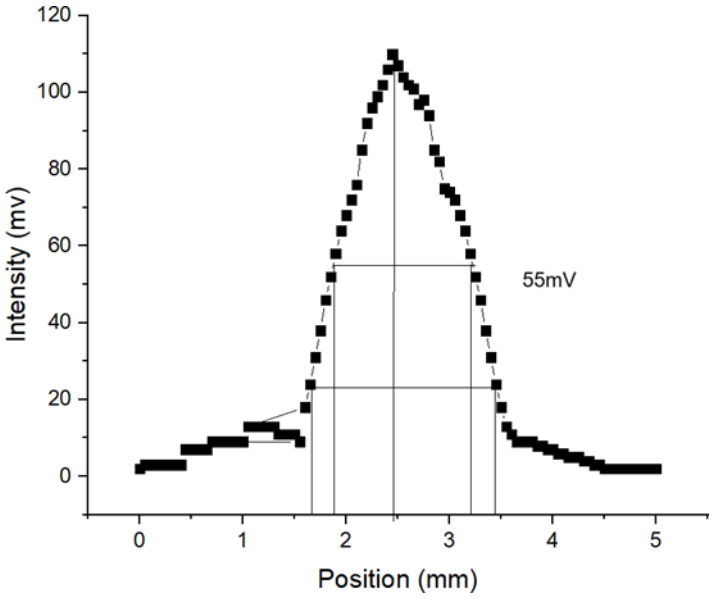

Figure 6 Intensity (mV) against Position (mm) for blue laser using dual-beam mode- mismatched thermal lens method.

Table 1 Experimental data for beam profiling of lasers using PPE setup.

Sample	Full width half max (FWHM)/mm	Spot size/mm	Spot radius/mm
Green laser	1.33	1.64	0.62
Blue laser	1.23	1.81	0.69

Table 2 Experimental data for beam profiling of lasers using dual-beam mode-mismatched thermal lens method.

Sample	Full width half max (FWHM)/mm	Spot size/mm	Spot radius/mm
Green laser	1.33	1.65	0.63
Blue laser	1.23	1.82	0.70

From the experimental results of the optimization of laser beam using PPE and dual- beam mode-mismatched thermal lens method, it is clearly seen that spot radius of the blue laser dan green laser are slightly bigger than spot radius using PPE setup. The deviation of the green laser using dual-beam mode-mismatched thermal lens method is 1.61% if compared to that of using PPE setup, whereas the deviation of blue laser using dual-beam mode- mismatched thermal lens method is 1.44% if compared to that of using PPE setup.

The deviation of the both lasers are less than 2%. Generally, the reflection of the laser beam will not cause any changes in spot radius. But experimentally, the deviations happened maybe due to the imperfection of the surface of the glass as the glass used in the experiment is normal glass, and it is not a standard refractive glass.

Determination of thermal diffusivity of standard liquid and with different concentrations using PPE setup with PVDF sensor

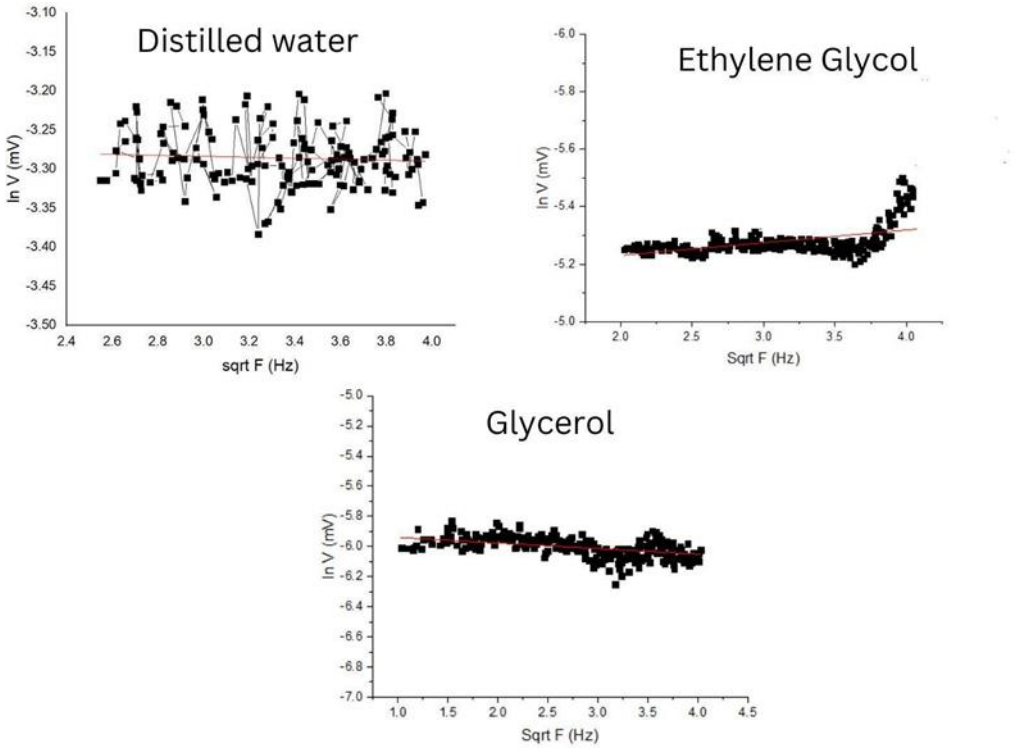

Figure 7 Graphs of ln V (mV) against Sqrt F (Hz) using PPE setup for blue laser on distilled water, ethylene glycol and glycerol.

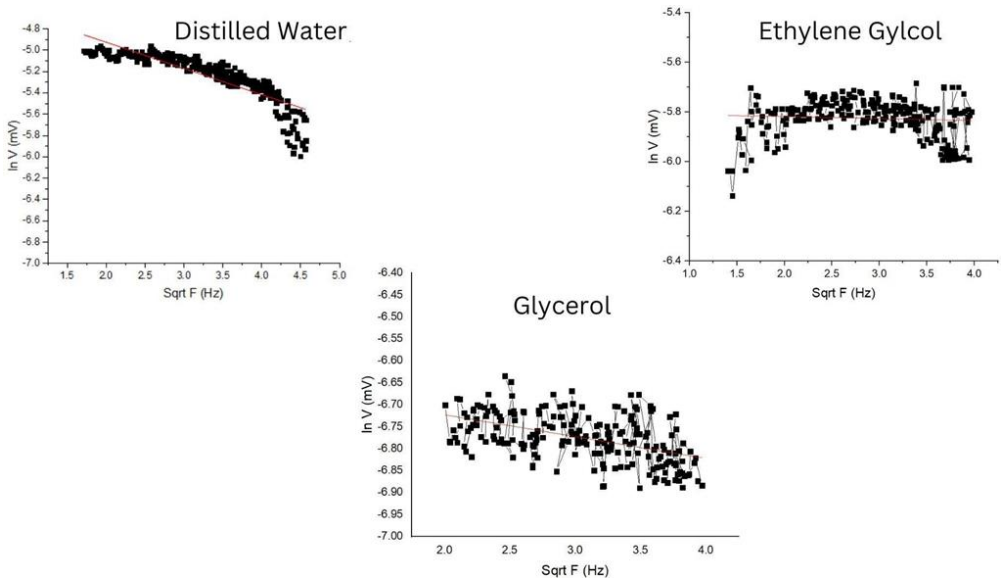

Figure 8 Graphs of ln V (mV) against Sqrt F (Hz) using PPE setup for green laser on distilled water, ethylene glycol and glycerol.

Table 3 Thermal diffusivity values of standard liquids using PPE setup for blue laser.

Sample	Experimental thermal diffusivity/x$10^{-7}$$m^2$$s^{-1}$	Theoretical thermal

	Blue laser					diffusivity/x10^{-7}m^{2}s^{-1}
	Distilled Water (ref)	Ethylene Glycol (ref)	Glycerol (ref)	Average	Deviation (%)	
Distilled Water	-	1.33±0.0426	1.35±0.0345	1.34±0.023	6.29	1.43
Ethylene Glycol	1.24±0.0346	-	1.35±0.0367	1.30±0.033	7.14	1.40
Glycerol	0.14±0.0347	0.11±0.0354	-	0.13±0.0353	8.33	0.12

Table 4 Thermal diffusivity values of standard liquids using PPE setup for green laser.

Sample	Experimental thermal diffusivity/x10^{-7}m^{2}s^{-1}					Theoretical thermal diffusivity/x10^{-7}m^{2}s^{-1}
	Green laser					
	Distilled Water (ref)	Ethylene Glycol (ref)	Glycerol (ref)	Average	Deviation (%)	
Distilled Water	-	1.13±0.0456	1.39±0.0425	1.26±0.0342	11.89	1.43
Ethylene Glycol	1.21±0.0443	-	1.25±0.0435	1.23±0.0234	12.14	1.40
Glycerol	0.15±0.0435	0.13±0.0432	-	0.14±0.0322	16.67	0.12

The results have proven that blue laser is more suitable to use in thermal diffusivity values finding which is similar to the result of the power laser as shown in Table 3 and Table 4. However, there are very less literature showing that the effect of the volume of the liquids to the change in thermal diffusivity. In order to further verify the justification that volume increase will not have major changes on thermal diffusivity, a comparison using same standard liquids with different volume is done.

Table 5 Comparison of thermal diffusivity values using same standard liquids with different volumes by using blue laser

Sample	Experimental thermal diffusivity/x10^{-7}m^{2}s^{-1}																			Theoretical thermal diffusivity /x10^{-7}m^{2}s^{-1}
	Blue laser																			
	Distilled Water (ref)							Ethylene Glycol (ref)							Glycerol (ref)							
	0.5 ml	1.0 ml	1.5 ml	2.0 ml	2.5 ml	Average	Deviation (%)	0.5 ml	1.0 ml	1.5 ml	2.0 ml	2.5 ml	Average	Deviation (%)	0.5 ml	1.0 ml	1.5 ml	2.0 ml	2.5 ml	Average	Deviation (%)	
Distilled Water	-	-	-	-	-	-	-	1.36 ±0.0 423	1.33 ±0.0 426	1.40 ±0.0 421	1.44 ±0.0 452	1.42 ±0.0 431	1. 39	2.8 0	1.32 ±0.0 322	1.35 ±0.0 345	1.36 ±0.0 321	1.33 ±0.0 311	1.32 ±0.0 351	1. 34	6.2 9	1.43
Ethylene Glycol	1.21 ±0.0 322	1.24 ±0.0 346	1.26 ±0.0 345	1.23 ±0.0 312	1.22 ±0.0 314	1. 23	11. 89	-	-	-	-	-	-	-	1.34 ±0.0 362	1.35 ±0.0 367	1.38 ±0.0 362	1.36 ±0.0 321	1.33 ±0.0 352	1. 35	3.5 7	1.40
Glycerol	0.12 ±0.0 323	0.14 ±0.0 347	0.16 ±0.0 354	0.13 ±0.0 341	0.16 ±0.0 342	0. 14	16. 67	0.12 ±0.0 362	0.11 ±0.0 357	0.14 ±0.0 352	0.12 ±0.0 342	0.13 ±0.0 322	0. 12	0.0 0	-	-	-	-	-	-	-	0.12

Table 6 Comparison of thermal diffusivity values using same standard liquids with different volumes by using green laser.

Sample	Experimental thermal diffusivity/x10^{-7}m^{2}s^{-1}																			Theoretical thermal diffusivity/ x10^{-7}m^{2}s^{-1}
	Green laser																			
	Distilled Water (ref)							Ethylene Glycol (ref)						Glycerol (ref)						
	0.5 ml	1.0 ml	1.5 ml	2.0 ml	2.5 ml	Average	Deviation (%)	0.5 ml	1.0 ml	1.5 ml	2.0 ml	2.5 ml	Average	Deviation (%)	0.5 ml	1.0 ml	1.5 ml	2.0 ml	2.5 ml	Average	Deviation (%)	
Distilled Water	-	-	-	-	-	-	-	1.12 ±0.432	1.13 ±0.456	1.35 ±0.453	1.34 ±0.462	1.35 ±0.451	1.26	11.89	1.37 ±0.422	1.39 ±0.425	1.38 ±0.412	1.36 ±0.432	1.35 ±0.442	1.31	8.39	1.43
Ethylene Glycol	1.20 ±0.421	1.21 ±0.443	1.24 ±0.452	1.26 ±0.432	1.23 ±0.452	1.23	12.14	-	-	-	-	-	-	-	1.25 ±0.423	1.25 ±0.435	1.26 ±0.453	1.28 ±0.432	1.24 ±0.443	1.26	10.0	1.40
Glycerol	0.12 ±0.423	0.15 ±0.435	0.14 ±0.453	0.15 ±0.423	0.12 ±0.441	0.14	16.67	0.15 ±0.442	0.13 ±0.432	0.15 ±0.312	0.14 ±0.421	0.15 ±0.413	0.14	16.67	-	-	-	-	-	-	-	0.12

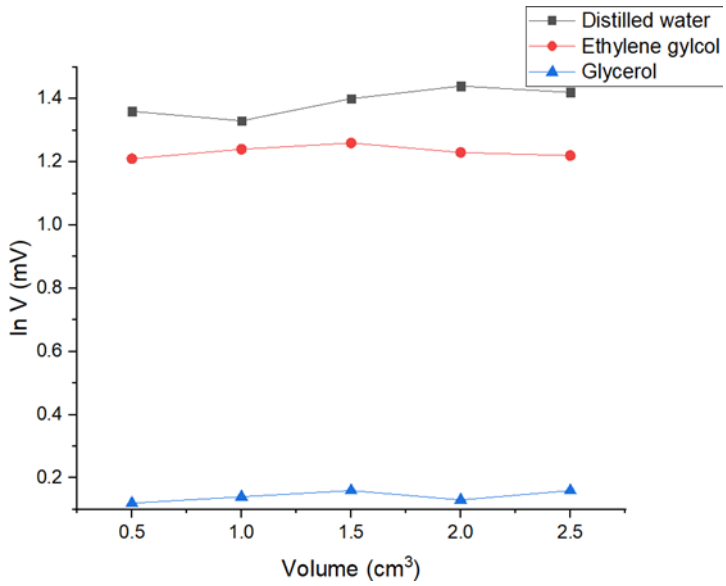

Figure 9 ln V against different volumes of standard liquid using blue laser.

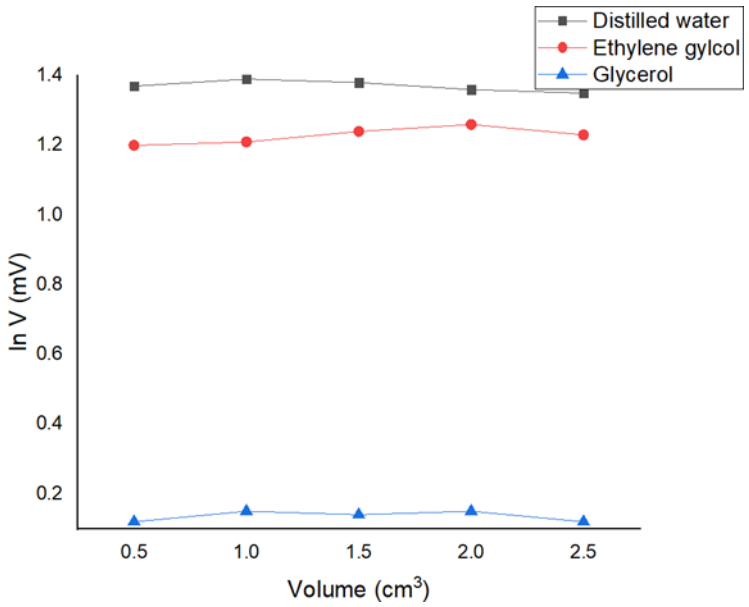

Figure 10 ln V against different volumes of standard liquid using green laser.

Blue laser showing almost similar trend over all the standard liquids with different volumes. It is further verified when the percentage of errors using blue laser is smaller than that of using green laser. Green laser, in the other hand, shows a fluctuating trend over all the standard liquids as the percentage of error is bigger if compared to blue laser of the same liquids. For example, the thermal diffusivity value of glycerol with ethylene glycol as reference, it is clearly seen that blue laser has most accurate reading which is 0.00% if compared to theoretical value whereas green laser has a deviation of 16.67% if compared to theoretical value.

Figure 9 and Figure 10, as example, ethylene glycol, they show the same trend that ln V increases when volume increases, but slightly decrease in the end of the graph. Generally, when

comparing across the Figure 9 and Figure 10, most of the ln V reading shows a decrease in the end of the graph, or when the volume is more than 1.5cm^3 and above.

This is because thermal conductivity generally decreases as the volume of a liquid increases due to the increased likelihood of molecular collisions and interactions within the larger volume. In a smaller volume, molecules are more densely packed, allowing for more frequent collisions and efficient transfer of thermal energy. When the volume increases, molecules have to travel greater distances on average before encountering another molecule. This results in a decrease in the frequency of collisions and, consequently, a reduction in thermal conductivity. Additionally, larger volumes may also exhibit greater molecular disorder or irregularities in molecular structure, further hindering the efficient transfer of thermal energy.

From Figure 9 and Figure 10, ln V increases at first when volume increases, and then drop when the volume increases gradually. This is due to the temperature gradient. When there is a temperature difference across a material, heat flows from regions of higher temperature to regions of lower temperature. This flow of heat creates a temperature gradient within the material. The rate at which heat flows through the material per unit area per unit temperature gradient is described by thermal conductivity. In most materials, thermal conductivity increases with increasing temperature, up to a certain point. This is due to various factors, such as increased molecular motion and collisions at higher temperatures, leading to more efficient transfer of thermal energy.

In simpler way to conclude, it is because when the volume increases, the laser power is not enough to let the heat to penetrate through the sample in a short interval time, resulting there is a temperature difference happening in the liquid of upper part and lower part, which is called temperature gradient.

Determination of thermal diffusivity of standard liquid and with different concentrations using PPE setup with photodiode sensor

The sample used in this study is in liquid form. PVDF sensor is not suitable to be used in dual-beam mode-mismatched due to its limitation of opaque property which not allows the laser beam to pass through. So, in order to overcome the problem, another sensor should be chosen. Photodiode sensor is the best sensor to be considered due to its cost and properties such as thermal stability as it can operate at high temperature until 150°C. This is important as the laser will generate heat when it hits on the surface of the sensor.

Photodiode sensor and PVDF sensor both can generate electrical signals as output, this is why PPE experiment is repeated so that to prove that photodiode sensor is suitable to use in the dual-beam mode-mismatched thermal lens method setup.

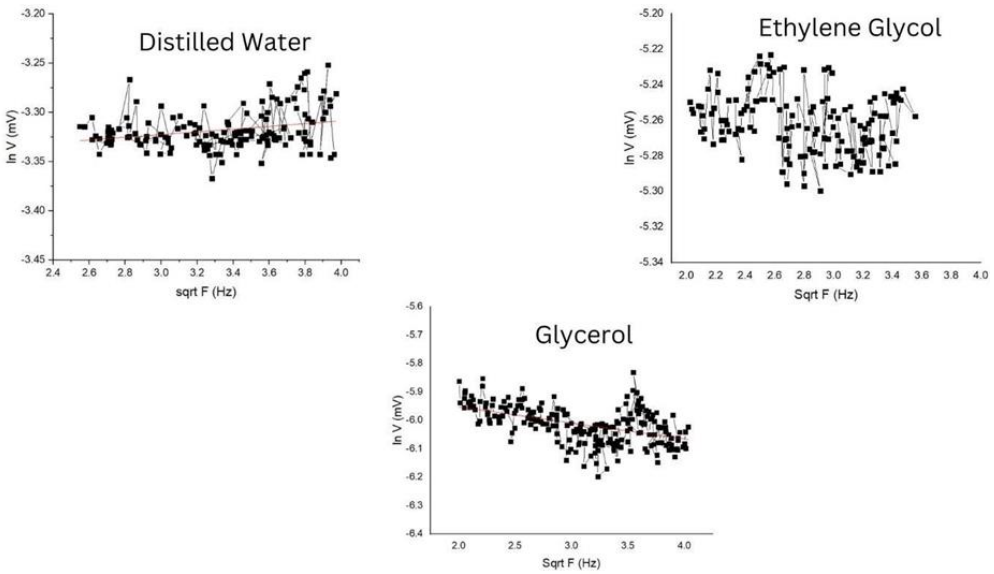

Figure 11 Graphs of ln V (mV) against Sqrt F (Hz) using PPE setup for blue laser on distilled water, ethylene glycol and glycerol using photodiode sensor.

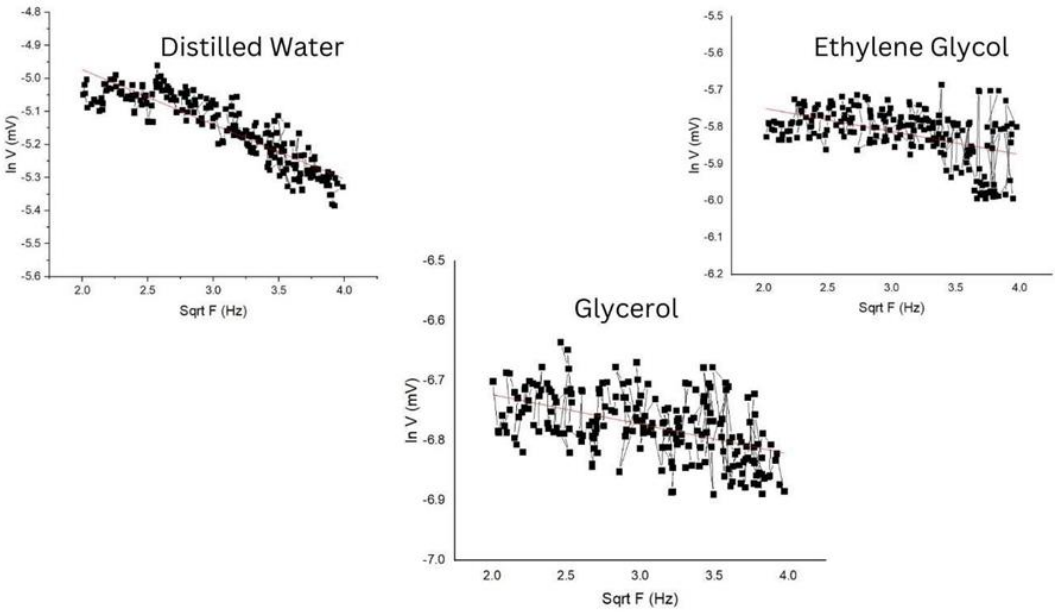

Figure 12 Graphs of ln V (mV) against Sqrt F (Hz) using PPE setup for green laser on distilled water, ethylene glycol and glycerol using photodiode sensor.

Table 7 Thermal diffusivity values of standard liquids using PPE setup with photodiode sensor.

Sample	Experimental thermal diffusivity/x$10^{-7}m^2s^{-1}$					Theoretical thermal diffusivity/x$10^{-7}m^2s^{-1}$
	Blue laser					
	Distilled Water (ref)	Ethylene Glycol (ref)	Glycerol (ref)	Average	Deviation (%)	
Distilled Water	-	1.37±0.0421	1.33±0.0345	1.35	5.59	1.43

Ethylene Glycol	1.34±0.0376	-	1.32±0.0387	1.33	5.00	1.40
Glycerol	0.14±0.0355	0.12±0.0332	-	0.13	8.33	0.12

Table 8 Thermal diffusivity values of standard liquids using PPE setup with photodiode sensor.

Sample	Experimental thermal diffusivity/x$10^{-7}m^2s^{-1}$					Theoretical thermal diffusivity/x$10^{-7}m^2s^{-1}$
	Green laser					
	Distilled Water (ref)	Ethylene Glycol (ref)	Glycerol (ref)	Average	Deviation (%)	
Distilled Water	-	1.33±0.0455	1.37±0.0434	1.35	5.59	1.43
Ethylene Glycol	1.24±0.0423	-	1.23±0.0432	1.24	11.42	1.40
Glycerol	0.14±0.0425	0.13±0.0411	-	0.14	16.67	0.12

From Table 7 and Table 8, blue laser has better experimental thermal diffusivity values as the overall deviations are much lesser than that of green laser as shown. The results have proven that blue laser is more suitable to use in thermal diffusivity values. This is similar to the findings show at Table 3 and Table 4.

In conclusion, blue laser is chosen as excitation laser due to its higher power and more stable output signal, and green laser as probe laser in the dual-beam mode-mismatched thermal lens method setup.

The PPE setup using photodiode sensor also used to study the thermal diffusivity values of different volumes so as to show that the similar output as using PVDF sensor.

Table 9 Comparison of thermal diffusivity values using same standard liquids with different volumes by using blue laser.

Sample	Experimental thermal diffusivity/x10^{-7}m^{2}s^{-1}																			Theoretical thermal diffusivity /x10^{-7}m^{2}s^{-1}
	Blue laser																			
	Distilled Water (ref)							Ethylene Glycol (ref)							Glycerol (ref)							
	0.5 ml	1.0 ml	1.5 ml	2.0 ml	2.5 ml	Average	Deviation (%)	0.5 ml	1.0 ml	1.5 ml	2.0 ml	2.5 ml	Average	Deviation (%)	0.5 ml	1.0 ml	1.5 ml	2.0 ml	2.5 ml	Average	Deviation (%)	
Distilled Water	-	-	-	-	-	-	-	1.37 ±0.0 423	1.37 ±0.0 421	1.42 ±0.0 421	1.40 ±0.0 452	1.37 ±0.0 431	1. 39	2.8 0	1.35 ±0.0 322	1.33 ±0.0 345	1.42 ±0.0 321	1.39 ±0.0 311	1.37 ±0.0 351	1. 37	4.2 0	1.43
Ethylene Glycol	1.30 ±0.0 322	1.34 ±0.0 346	1.31 ±0.0 345	1.33 ±0.0 312	1.29 ±0.0 314	1. 31	6,4 3	-	-	-	-	-	-	-	1.34 ±0.0 362	1.32 ±0.0 367	1.38 ±0.0 362	1.32 ±0.0 321	1.33 ±0.0 352	1. 34	4.2 9	1.40
Glycerol	0.12 ±0.0 323	0.14 ±0.0 347	0.16 ±0.0 354	0.13 ±0.0 341	0.11 ±0.0 342	0. 13	8.3 3	0.11 ±0.0 362	0.12 ±0.0 357	0.16 ±0.0 352	0.14 ±0.0 342	0.12 ±0.0 322	0. 13	8.3 3	-	-	-	-	-	-	-	0.12

Table 10 Comparison of thermal diffusivity values using same standard liquids with different volumes by using green laser.

Sample	Experimental thermal diffusivity/x10^{-7}m^{2}s^{-1}																			Theoretical thermal diffusivity /x10^{-7}m^{2}s^{-1}
	Green laser																			
	Distilled Water (ref)							Ethylene Glycol (ref)						Glycerol (ref)						
	0.5 ml	1.0 ml	1.5 ml	2.0 ml	2.5 ml	Average	Deviation (%)	0.5 ml	1.0 ml	1.5 ml	2.0 ml	2.5 ml	Average	Deviation (%)	0.5 ml	1.0 ml	1.5 ml	2.0 ml	2.5 ml	Average	Deviation (%)	
Distilled Water	-	-	-	-	-	-	-	1.30 ±0.432	1.33 ±0.456	1.35 ±0.453	1.32 ±0.462	1.32 ±0.451	1.32	7.69	1.34 ±0.422	1.37 ±0.425	1.38 ±0.412	1.35 ±0.432	1.34 ±0.442	1.36	4.90	1.43
Ethylene Glycol	1.22 ±0.421	1.24 ±0.443	1.26 ±0.452	1.23 ±0.432	1.23 ±0.452	1.24	11.43	-	-	-	-	-	-	-	1.20 ±0.423	1.23 ±0.435	1.32 ±0.453	1.28 ±0.432	1.29 ±0.443	1.26	10.0	1.40
Glycerol	0.12 ±0.423	0.14 ±0.435	0.14 ±0.453	0.13 ±0.423	0.12 ±0.441	0.13	7.69	0.11 ±0.442	0.13 ±0.432	0.15 ±0.312	0.14 ±0.421	0.13 ±0.413	0.13	7.69	-	-	-	-	-	-	-	0.12

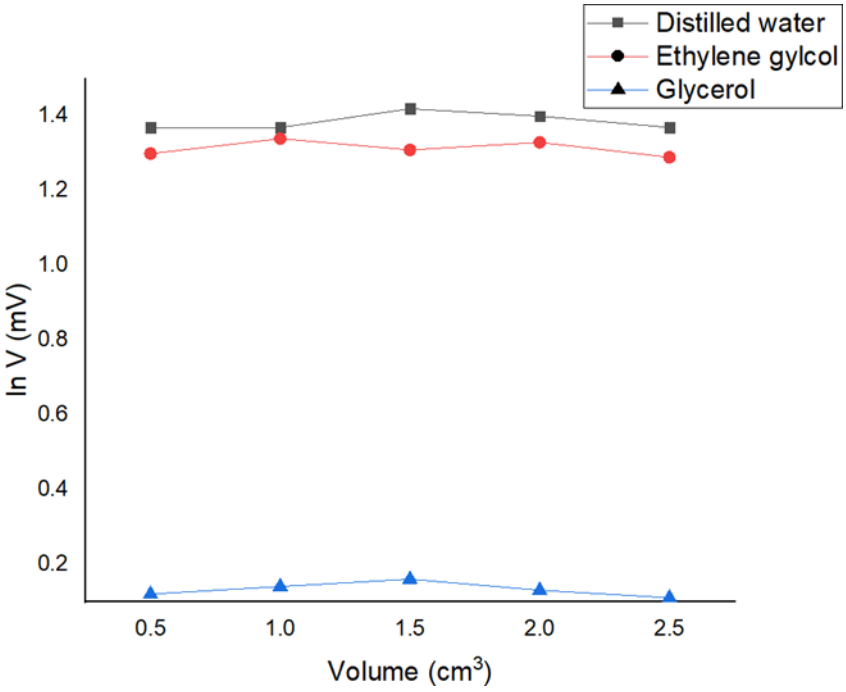

Figure 13 ln V against different volumes of standard liquid using blue laser.

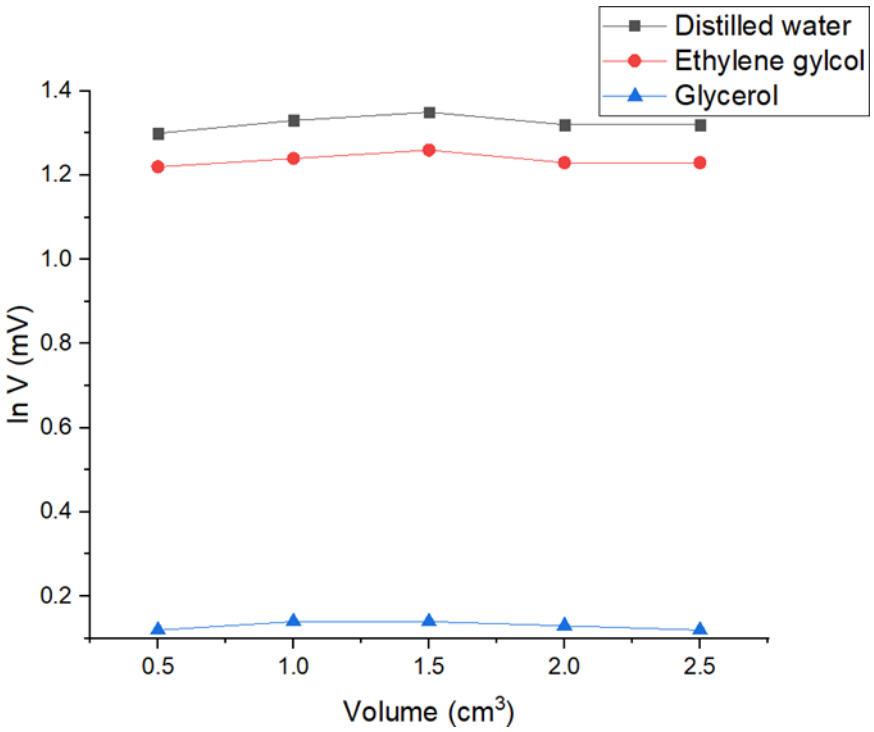

Figure 14 ln V against different volumes of standard liquid using green laser.

From Table 9 and Table 10, when the sensor changed from PVDF to photodiode sensor, it shows the similar trend where blue laser shows the better thermal diffusivity values. It is further verified when comparison across blue and green lasers when volume increases, there will be showing a decrease trend in the end of the graphs which is similar to that of using PVDF sensor. Hence, with these results, photodiode sensor is chosen to be the sensor in the dual- beam mode-

mismatched thermal lens method. This is because the results obtained by using photodiode sensor is almost the same as by using the PVDF sensor.

However, in order to maintain the consistent results, the optical distance travelled by the laser beam, especially the excitation beam must be as same as the distance in PPE setup. This is because when the optical distance changes, the transmission of the light also changes, in which will affect the heat of the light that the heat energy of the light source will be lost to surroundings.

Determination of thermal diffusivity of standard liquids and with different concentrations using dual-beam mode-mismatched thermal lens method with photodiode sensor

The purpose of repeating the experiment using dual-beam mode-mismatched thermal lens method is to verify the validity of the dual-beam mode-mismatched thermal lens method setup as PPE setup using photodiode sensor as a reference setup. This is a precaution step as to further ensure the data obtained and analyzed will be valid and consistent to the theoretical values.

Table 11 Thermal diffusivity values of standard liquids using dual-beam mode-mismatched thermal lens method

Sample	Experimental thermal diffusivity/x10^{-7}m^{2}s^{-1}					Theoretical thermal diffusivity/x10^{-7}m^{2}s^{-1}
	Distilled Water (ref)	Ethylene Glycol (ref)	Glycerol (ref)	Average	Deviation (%)	
Distilled Water	-	1.38±0.0321	1.39±0.0344	1.39	2.80	1.43
Ethylene Glycol	1.30±0.0431	-	1.29±0.0392	1.30	5.00	1.40
Glycerol	0.13±0.0411	0.12±0.0409	-	0.13	7.69	0.12

Table 12 Thermal diffusivity values of the standard liquids.

Sample	Experimental thermal diffusivity/x10^{-7}m^{2}s^{-1}			Theoretical thermal diffusivity/x10^{-7}m^{2}s^{-1}
	PPE (PVDF Sensor)	PPE (Photodiode sensor)	Dual-beam mode-mismatched thermal lens method	
Distilled water	1.34	1.35	1.39	1.43

Ethylene glycol	1.30	1.33	1.30	1.40
Glycerol	0.13	0.13	0.13	0.12

From Table 11, it is clearly seen that the deviations from dual-beam mode-mismatched thermal lens method show a better result if compared to all the setups and it is the nearest to the theoretical as shown in Table 12. This is because dual-beam mode-mismatched thermal lens method is a powerful tool for studying the thermal and optical properties of materials with high sensitivity and versatility.

The high sensitivity of the setup is due to the mode-mismatched configuration. This is because mode mismatching can optimize the interaction between the beams and the sample, thereby increasing sensitivity to changes induced by the pump beam or known as excitation beam. Mode mismatching also enable the two beam sources to have a slight gap which is less than 1.5°. This gap is extremely crucial because by separating the pump and probe beams, this setup can detect subtle changes induced by the pump beam without interference from the probe beam and vice versa. This separation enhances sensitivity to changes in the sample.

Since the thermal diffusivity values obtained using dual-beam mode-mismatched thermal lens method is almost the same with the PPE setup, therefore the setup is continued to use for determining the thermal diffusivity values of graphene oxide solutions.

Determination of thermal diffusivity of different concentration of GO using dual-beam mode-mismatched thermal lens method

The thermal diffusivity of graphene oxide (GO) can vary depending on several factors, including concentration, synthesis method, and experimental conditions. Generally, as the concentration of graphene oxide increases, the thermal diffusivity tends to decrease due to increased scattering of phonons (quasiparticles representing the quantized mechanical vibrations of the crystal lattice) at higher concentrations.

In order to determine thermal diffusivity of GO by using different concentrations, a solution of 100CC distilled water is mixed with 1g of GO powder to make the GO solutions into different concentrations as 0.5mg/ml, 1.0mg/ml, 1.5mg/ml, 2.0mg/ml and 2.5mg/ml.

Once the solutions are ready, the experiment is started by pouring the solution into the container to start the experiment.

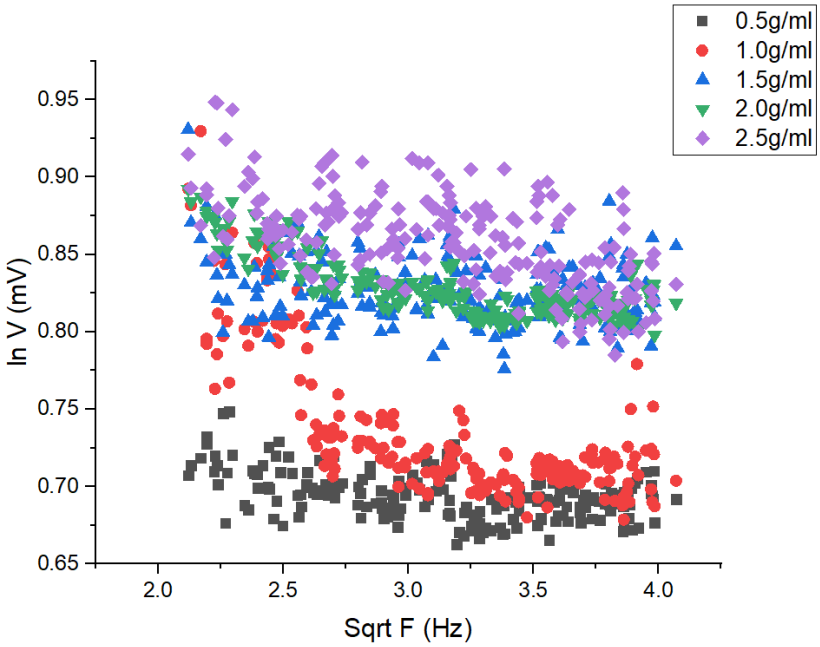

Figure 15 Dependence of amplitude signal as function of Sqrt Frequency, F of GO with at different concentration

From Figure 15, it shows that when the concentration ratio g/ml increases, the amplitude signal of voltage higher, resulting in an increment of the slope of graph (ln V/sqrt F) as summarized shown in Table 13 and Figure 16.

Table 13 Thermal diffusivity of GO with different concentrations.

Concentration/ g/ml	Experimental Thermal Diffusivity/ $x10^{-7}m^2s^{-1}$
0.5	0.14±0.013
1.0	0.15±0.013
1.5	0.18±0.012
2.0	0.21±0.016
2.5	0.24±0.015

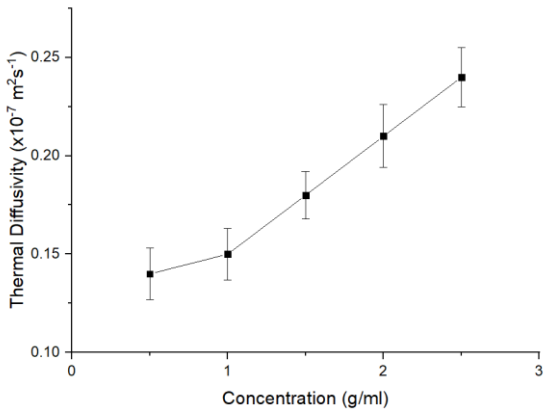

Figure 16 Graph of different concentrations against thermal diffusivity.

From Table 13, it is clearly noticed that when the particle concentration of the GO solutions increases, thermal diffusivity also increases [15]. As predicted by the thermal equilibrium model, the nanofluid's decreased specific heat capacity explains the increase in thermal diffusivity [8].

As the concentration of nanoparticles increases, so does the specific heat capacity. The observed enhancement of the thermal diffusivity is a result of both a drop in specific heat capacity and an increase in thermal conductivity[16]. Additionally, when the concentration of nanoparticles increases, optical absorption rises as well, improving thermal diffusivity [17-18].

Increasing the concentration of graphene oxide can have a significant impact on the thermal diffusivity of materials. Several studies provide insights into how changes in graphene oxide concentration influence thermal properties. For instance, research on graphene-based lubricants indicates that the thermal conductivity and viscosity of graphene lubricants increase with higher graphene concentrations [19]. Similarly, in composite materials, the thermal conductivity can increase with the rising content of reduced graphene oxide [20].

Moreover, the addition of functionalized graphene oxide to materials like polyetherimide has been shown to enhance thermal conductivity [21]. However, it is essential to note that the relationship between graphene oxide concentration and thermal diffusivity may not always follow a linear trend. Studies on dispersions of silicon oxide nanoparticles suggest that the thermal diffusivity can pass through a minimum threshold with increasing concentrations [6].

Furthermore, the thermal diffusivity of graphene composites can be influenced by the quantity of introduced graphene, with differences in thermal diffusivity observed between different directions as the graphene content increases [22]. Additionally, the thermal conductivity of nanofluids containing graphene oxide nanosheets can be significantly enhanced with higher loading levels [23].

The decrease in specific heat capacity with increasing graphene nanoparticle concentration, as observed in studies [24], can explain the increase in thermal diffusivity. When graphene nanoparticles are suspended in a fluid, the specific heat capacity of the suspension decreases as the nanoparticle concentration rises. This reduction in specific heat capacity is attributed to the lower heat storage capacity of the graphene nanoparticle suspension compared to the base fluid. Consequently, the decrease in specific heat capacity contributes to the increase in thermal diffusivity of the material, as noted in the research on graphene nanofluids [25]. The enhanced thermal properties of graphene dispersions, further support the notion that changes in specific heat capacity due to graphene concentration variations can influence thermal diffusivity.

CONCLUSION

This study successfully shown the thermal diffusivity measurement of standard liquid and different concentrations by using PPE setup with PVDF sensors and photodiode sensor and also by using dual-beam mode-mismatched thermal lens setup. When the particle concentration increases, thermal diffusivity increases. However, when the volume kept increasing, it will be affected due to presence of the temperature gradient.

REFERENCES

[1] J. P. Gordon, R. C. C. Leite, R. S. Moore, S. P. S. Porto, and J. R. Whinnery, “Long-Transient Effects in Lasers with Inserted Liquid Samples,” *J. Appl. Phys.*, vol. 36, no. 1, pp. 3–8, Jan. 1965, doi: 10.1063/1.1713919.

[2] R. Zamiri *et al.*, “Thermal diffusivity measurement of silver nanofluid by thermal lens technique,” *J. Laser Appl.*, vol. 23, no. 4, p. 042002, Nov. 2011, doi: 10.2351/1.3622205.

[3] E. Shahriari, M. Moradi, and M. Raeisi, “An experimental study of thermal diffusivity of Au nanoparticles: effects of concentration particle size,” *J. Theor. Appl. Phys.*, vol. 10, no. 4, pp. 259–263, Dec. 2016, doi: 10.1007/s40094-016-0224-x.
[4] S. E. Bialkowski and A. Mandelis, “*Photothermal Spectroscopy Methods for Chemical Analysis*,” *Phys. Today*, vol. 49, no. 10, pp. 76–76, Oct. 1996, doi: 10.1063/1.2807813.
[5] J. Shen, A. J. Soroka, and R. D. Snook, “A model for cw laser induced mode-mismatched dual-beam thermal lens spectrometry based on probe beam profile image detection,” *J. Appl. Phys.*, vol. 78, no. 2, pp. 700–708, July 1995, doi: 10.1063/1.360329.
[6] V. R. Khabibullin, L. O. Usoltseva, I. V. Mikheev, and M. A. Proskurnin, “Thermal Diffusivity of Aqueous Dispersions of Silicon Oxide Nanoparticles by Dual-Beam Thermal Lens Spectrometry,” *Nanomaterials*, vol. 13, no. 6, p. 1006, Mar. 2023, doi: 10.3390/nano13061006.
[7] D. P. Singh, C. E. Herrera, B. Singh, S. Singh, R. K. Singh, and R. Kumar, “Graphene oxide: An efficient material and recent approach for biotechnological and biomedical applications,” *Mater. Sci. Eng. C*, vol. 86, pp. 173–197, May 2018, doi: 10.1016/j.msec.2018.01.004.
[8] V. M. Lenart, N. G. C. Astrath, R. F. Turchiello, G. F. Goya, and S. L. Gómez, “Thermal diffusivity of ferrofluids as a function of particle size determined using the mode-mismatched dual-beam thermal lens technique,” *J. Appl. Phys.*, vol. 123, no. 8, p. 085107, Feb. 2018, doi: 10.1063/1.5017025.
[9] L. G. Rodriguez, P. Iza, and J. L. Paz, “Study of dependence between thermal diffusivity and sample concentration measured by means of frequency-resolved thermal lens experiment,” *J. Nonlinear Opt. Phys. Mater.*, vol. 25, no. 02, p. 1650022, June 2016, doi: 10.1142/S0218863516500223.
[10] K. Chen, “Advances in Perovskite Photodiodes: Material and Device Innovations,” *J. Photonic Mater.*, vol. 15, no. 2, 2023.
[11] K. S. Novoselov and et. al., “Electric Field Effect in Atomically Thin Carbon Films,” *Phys Rev Lett*, vol. 404, 2000.
[12] E. M. Chua, J. Shimeta, D. Nugegoda, P. D. Morrison, and B. O. Clarke, “Assimilation of Polybrominated Diphenyl Ethers from Microplastics by the Marine Amphipod, *Allorchestes Compressa*,” *Environ. Sci. Technol.*, vol. 48, no. 14, pp. 8127–8134, July 2014, doi: 10.1021/es405717z.
[13] A. B. Silva, A. S. Bastos, C. I. L. Justino, J. P. Da Costa, A. C. Duarte, and T. A. P. Rocha-Santos, “Microplastics in the environment: Challenges in analytical chemistry - A review,” *Anal. Chim. Acta*, vol. 1017, pp. 1–19, Aug. 2018, doi: 10.1016/j.aca.2018.02.043.
[14] W. I. Liu *et al.*, “A novel comprehensive experimental study concerned graphene oxide nanoparticles dispersed in water: Synthesise, characterisation, thermal conductivity measurement and present a new approach of RLSF neural network,” *Int. Commun. Heat Mass Transf.*, vol. 109, p. 104333, Dec. 2019, doi: 10.1016/j.icheatmasstransfer.2019.104333.
[15] J. L. Jiménez-Pérez, G. López-Gamboa, J. F. Sánchez-Ramírez, Z. N. Correa-Pacheco, A. Netzahual-Lopantzi, and A. Cruz-Orea, “Thermal Diffusivity Dependence with Highly Concentrated Graphene Oxide/Water Nanofluids by Mode-Mismatched Dual-Beam Thermal Lens Technique,” *Int. J. Thermophys.*, vol. 42, no. 7, p. 107, July 2021, doi: 10.1007/s10765-021-02861-6.
[16] J. John, L. Thomas, B. Rajesh Kumar, A. Kurian, and S. D. George, “Shape dependent heat transport through green synthesized gold nanofluids,” *J. Phys. Appl. Phys.*, vol. 48, no. 33, p. 335301, Aug. 2015, doi: 10.1088/0022-3727/48/33/335301.
[17] R. Herrera-Aquino, J. L. Jiménez-Pérez, D. C. Altamirano-Juárez, G. López-Gamboa, Z. N. Correa-Pacheco, and R. Carbajal-Valdéz, “Green Synthesis of Silver Nanoparticles Contained in Centrifuged Citrus Oil and Their Thermal Diffusivity Study by Using Thermal Lens Technique,” *Int. J. Thermophys.*, vol. 40, no. 1, p. 3, Jan. 2019, doi: 10.1007/s10765-018-2466-0.
[18] M. Ramya, T. K. Nideep, V. P. N. Nampoori, and M. Kailasnath, “Particle size and concentration effect on thermal diffusivity of water-based ZnO nanofluid using the dual-beam thermal lens technique,” *Appl. Phys. B*, vol. 125, no. 9, p. 181, Sept. 2019, doi: 10.1007/s00340-019-7294-9.

[19] Z. Cai, M. Tian, and G. Zhang, “Experimental Study on the Flow and Heat Transfer of Graphene-Based Lubricants in a Horizontal Tube,” *Processes*, vol. 8, no. 12, p. 1675, Dec. 2020, doi: 10.3390/pr8121675.
[20] J. Wilk, R. Smusz, R. Filip, G. Chmiel, and T. Bednarczyk, “Experimental investigations on graphene oxide/rubber composite thermal conductivity,” *Sci. Rep.*, vol. 10, no. 1, p. 15533, Sept. 2020, doi: 10.1038/s41598-020-72633-z.
[21] Y. Hwang, Y. Heo, Y. Yoo, and J. Kim, “The addition of functionalized graphene oxide to polyetherimide to improve its thermal conductivity and mechanical properties: ENHANCED PROPERTIES OF THE FUNCTIONALIZED GO/PEI COMPOSITES,” *Polym. Adv. Technol.*, vol. 25, no. 10, pp. 1155–1162, Oct. 2014, doi: 10.1002/pat.3369.
[22] P. Rutkowski, P. Klimczyk, L. Jaworska, L. Stobierski, and A. Dubiel, “Thermal properties of pressure sintered alumina–graphene composites,” *J. Therm. Anal. Calorim.*, vol. 122, no. 1, pp. 105–114, Oct. 2015, doi: 10.1007/s10973-015-4694-x.
[23] W. Yu, H. Xie, and D. Bao, “Enhanced thermal conductivities of nanofluids containing graphene oxide nanosheets,” *Nanotechnology*, vol. 21, no. 5, p. 055705, Feb. 2010, doi: 10.1088/0957-4484/21/5/055705.
[24] K. Ramesh, J. Ponnusamy, and P. Periasamy, “Synthesis of Antimicrobial and Antioxidant Zinc Oxide Hydrogel for Drug Delivery Applications,” *Indones. J. Chem.*, vol. 24, no. 6, p. 1615, Dec. 2024, doi: 10.22146/ijc.85663.
[25] M. R. Rodríguez-Laguna *et al.*, “Mechanisms behind the enhancement of thermal properties of graphene nanofluids,” *Nanoscale*, vol. 10, no. 32, pp. 15402–15409, 2018, doi: 10.1039/C8NR02762E.